

Electronic supplementary information (ESI):  
**A sensitive calorimetric technique to study energy  
(heat) exchange at the nano-scale**

Luca Basta<sup>1,†</sup>, Stefano Veronesi<sup>1,†</sup>, Yuya Murata<sup>1</sup>, Zoé Dubois<sup>1</sup>, Neeraj Mishra<sup>2,3</sup>,  
Filippo Fabbri<sup>2,3</sup>, Camilla Coletti<sup>2,3</sup>, and Stefan Heun<sup>1</sup>

<sup>1</sup>*NEST, Istituto Nanoscienze-CNR and Scuola Normale Superiore, Piazza S. Silvestro 12, 56127  
Pisa, Italy*

<sup>2</sup>*Center for Nanotechnology Innovation @ NEST, Istituto Italiano di Tecnologia, Piazza S.  
Silvestro 12, 56127 Pisa, Italy*

<sup>3</sup>*Graphene Labs, Istituto Italiano di Tecnologia, Via Morego 30, 16163 Genova, Italy*

<sup>†</sup>luca.basta1@sns.it

<sup>†</sup>stefano.veronesi@nano.cnr.it

## Gold film thermometer

The physical support of the sensor is a  $\sim 300$   $\mu\text{m}$ -thick substrate of silicon whose top face has been oxidized to obtain a 280 nm layer of  $\text{SiO}_2$  as an electrical and thermal insulation. A thin layer of 5 nm of titanium is deposited on the substrate in order to allow the proper sticking of an upper 20 nm layer of gold. Both gold and titanium have been deposited *via* metal sputtering. Gold has been chosen as metal for the thermometer because of its large resistance temperature coefficient. Moreover, it has good thermal and electrical conductivities, and low chemical reactivity which reduces the amount of impurities collected from the environment. Finally, a high-quality monolayer of CVD-grown polycrystalline graphene is transferred onto the gold layer. As a last step, titanium is evaporated in-situ on the graphene to functionalize the surface (see Fig. S1).



Figure S1: Scheme of the sensor (dimensions not to scale). From the top: Ti evaporated (dark gray islands), graphene monolayer (black and white), Au layer (yellow), Ti layer for proper sticking (gray), SiO<sub>2</sub> insulator layer (light blue), Si substrate (dark blue).

## Thermometer Calibration

In order to check the repeatability and the stability of the thermometers, we performed calibrations after several manipulations of the sample. We mounted and demounted it for three times, and we repeated the measurement before and after the thermometer had been staying idle in UHV for several days. The resulting calibration curves are shown in Fig. S2. All curves are linear, as expected, and their slopes  $R_0 \cdot \alpha = dR/dT$  span the range  $(2.1 - 2.8) \cdot 10^{-3} \text{ K}^{-1}$ . Overall, the values of  $\alpha$  show a good agreement to within  $\sim 15\%$ .

This calibration procedure was repeated for samples after each fabrication step (only the gold sensor, Au with the graphene layer, and with the titanium deposited on the graphene). The resulting values of the temperature coefficient of resistance  $\alpha$  and the electrical resistivity  $\rho$  are listed in Table S1, together with the weighted average values and the values of bulk Au known from literature (see Ref. [5]).

The  $\alpha_i$  values measured for only the Au thermometer (without [samples 1,2] or with [samples G1-3] MLG) show a good mutual agreement, with the value for sample G3 slightly lower, which will be discussed below. Comparing the average values of  $\alpha_i$  (without Ti) and  $\alpha_f$  (with Ti, after adsorption and desorption of  $D_2$ ), we notice that the latter values are consistently smaller. This is likely due to the Ti overlayer on the graphene which modifies the temperature coefficient of the resistance, resulting in a modification of the parameter. In particular, considering the Ti layer and the Au with MLG as two parallel layers, the resulting temperature coefficient of resistance  $\alpha_f$  is lower than  $\alpha_i$ . On the other hand, the discrepancy between  $\alpha_i$  of sample G3 and the other samples is not completely understood, but could be due to some inhomogeneities of the Ti layer underneath the Au layer. In fact, the value of  $\alpha_i$  for sample G3 is very close to the values of  $\alpha_f$ , which derive from the addition of a new Ti layer. We want to remind that the Au thermometer is not bulk, but a 20 nm thin film, where the interfaces play a major role. However, these surface modifications are simply an effect of the preparation of the device and do not affect the

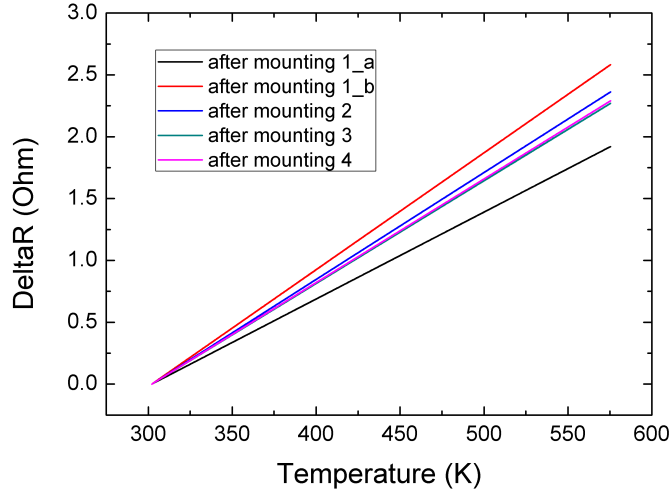


Figure S2: Resistance variation vs. temperature for five different calibration runs on the same sample (Au with MLG). Between mounting 1\_a and 1\_b the sample has been stored for several days in UHV.

validity of the procedure, because we have performed a complete calibration of each device before its use as a sensor.

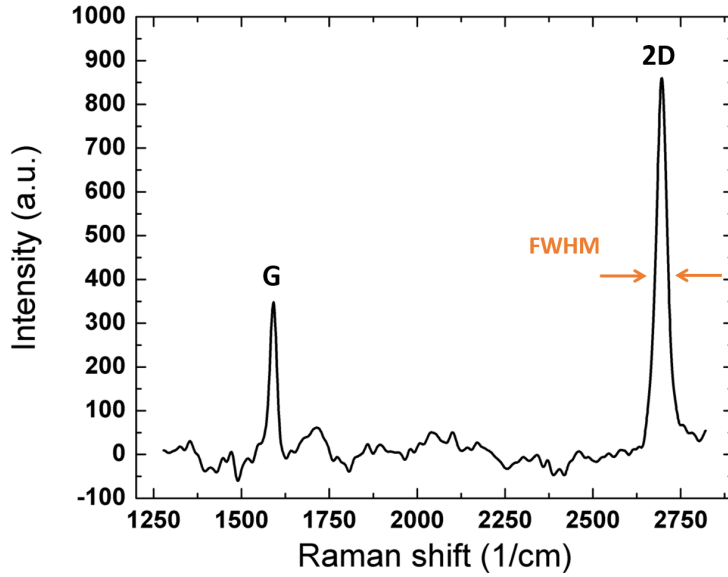
Regarding the electrical resistivity of the sensors, all measured values are in good agreement within the error bars. This demonstrates a good repeatability of the experiment. Variations of  $\alpha$  and  $\rho$  from the tabulated literature bulk values ( $\alpha = 3.4 \cdot 10^{-3} \text{ K}^{-1}$ ,  $\rho = 2.44 \cdot 10^{-8} \text{ } \Omega\text{m}$ ) [5] are expected [2] because we are not considering a gold bulk layer and an isolated system, but we have a corrugated, sputtered gold layer sandwiched between a Ti layer underneath and a Ti-MLG layer on top. Therefore, surface and interface corrugation can sensibly affect the transport properties of a 20 nm-thin layer of gold.

Sample	$R_0$ ( $\Omega$ )	$\alpha_i$ ( $\text{K}^{-1}$ )	$\alpha_f$ ( $\text{K}^{-1}$ )	$\rho_i$ ( $\Omega\text{m}$ )	$\rho_f$ ( $\Omega\text{m}$ )
1	2.96	$(2.8 \pm 0.2) \cdot 10^{-3}$	-	$(3.0 \pm 0.4) \cdot 10^{-8}$	-
2	3.57	$(2.4 \pm 0.3) \cdot 10^{-3}$	-	$(3.6 \pm 0.5) \cdot 10^{-8}$	-
G1	2.95	$(2.6 \pm 0.2) \cdot 10^{-3}$	$(2.0 \pm 0.4) \cdot 10^{-3}$	$(2.9 \pm 0.4) \cdot 10^{-8}$	$(3.5 \pm 0.4) \cdot 10^{-8}$
G2	2.79	$(2.8 \pm 0.5) \cdot 10^{-3}$	$(1.7 \pm 0.3) \cdot 10^{-3}$	$(3.2 \pm 0.4) \cdot 10^{-8}$	$(3.6 \pm 0.5) \cdot 10^{-8}$
G3	3.31	$(1.7 \pm 0.2) \cdot 10^{-3}$	$(1.8 \pm 0.2) \cdot 10^{-3}$	$(3.7 \pm 0.5) \cdot 10^{-8}$	$(3.6 \pm 0.5) \cdot 10^{-8}$
average (with G3)		$(2.4 \pm 0.4) \cdot 10^{-3}$	$(1.8 \pm 0.3) \cdot 10^{-3}$	$(3.2 \pm 0.4) \cdot 10^{-8}$	$(3.6 \pm 0.4) \cdot 10^{-8}$
(without G3)		$(2.7 \pm 0.1) \cdot 10^{-3}$			
literature (bulk)		$3.4 \cdot 10^{-3}$		$2.44 \cdot 10^{-8}$	

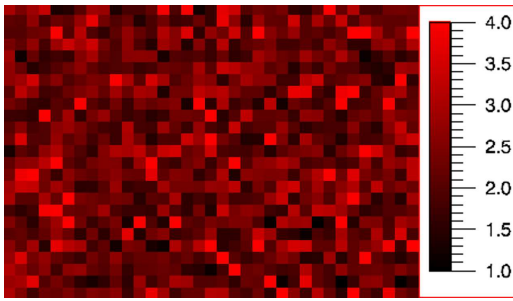
Table S1: Comparison of temperature coefficients of resistance  $\alpha$  and electrical resistivity  $\rho$ . Samples 1 and 2 refer to gold thermometer only, while samples G1-3 refer to gold thermometer plus graphene.  $\alpha_i$  and  $\rho_i$  are measured for only Au thermometer with or without MLG, while  $\alpha_f$  and  $\rho_f$  are measured for the Au thermometer with Ti-MLG.

## Raman Spectroscopy

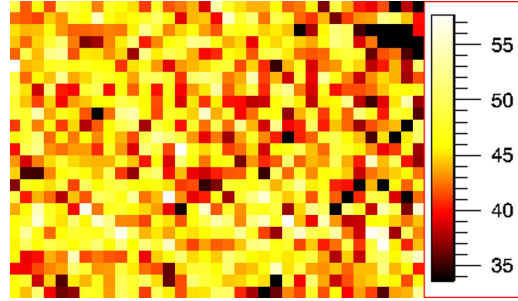
We performed Raman spectroscopy and mapping (see references [1, 4] for details) on our samples, using a Renishaw confocal microscope with a  $100\times$  objective (NA 0.85) equipped with a 532 nm laser as excitation source. The laser power is 1 mW in order to have a spot size of  $1 \mu\text{m}$ . The scan area is  $35 \times 25 \mu\text{m}^2$ , with 875 pixels, and a lateral pixel size of  $1 \mu\text{m}$ . Figure S3(a) shows a typical spectrum. The absence of a detectable  $D$  peak at  $\sim 1350 \text{ cm}^{-1}$ , which is related to the presence of defects in graphene, indicates the high quality of the transferred graphene. The intensity of the  $2D$  peak (at  $\sim 2690 \text{ cm}^{-1}$ ) is around 2 times higher than the intensity of the  $G$  peak (at  $\sim 1580 \text{ cm}^{-1}$ ). Figure S3(b) shows a Raman intensity ratio map, where each pixel gives the ratio between the intensity of the  $2D$  peak vs the  $G$  peak. The Full Width at Half Maximum (FWHM) of the  $2D$  peak is plotted in Figure S3(c), with an average value of  $46 \text{ cm}^{-1}$ . These two maps, the  $2D/G$  ratio and the FWHM of the  $2D$  peak, confirm that the sample is indeed monolayer graphene. Furthermore, they highlight the lateral homogeneity of the graphene.



(a)



(b)



(c)

Figure S3: (a) Raman spectrum of the graphene used in our devices, showing the expected  $G$  and  $2D$  peaks for monolayer graphene. (b) Raman intensity ratio map: each pixel gives the ratio between the intensity of the  $2D$  peak vs the  $G$  peak. (c) Raman map showing the FWHM (in  $\text{cm}^{-1}$ ) of the  $2D$  peak.

## Heat capacity calculation

The device is composed of several layers, and the most important are: the substrate, the temperature sensor, and the sample (Ti-MLG). We can contemplate two different limiting scenarios during the hydrogen adsorption: (a) the sensor is thermally decoupled from the substrate, or (b) the substrate and the sensor are fully thermalized. These two scenarios give, in our experimental conditions, an upper bound for the temperature increase of around

5 K and a lower bound of around 0.7 mK, respectively. Of course we can expect that the real  $\Delta T$  will be somewhere in between these two extreme values.

Further consideration of the thermalization behaviour of these devices leads to the expectation that three time scales will be involved: (i) a short one, related to the sample and thermometer thermalization, (ii) an intermediate one, related to the substrate thermalization, and (iii) a long one, related to the thermalization towards the environment (sample holder). In order to experimentally verify this, we heated the sample for a short time with a known thermal power, then we switched off the heating and monitored the cooling process. As expected, the cooling curve can be described as the sum of three exponential decays with very distinct time scales, where the shortest decay time corresponds to the thermometer thermalization. Table S2 lists the characteristic decay times obtained from this analysis of experimental data.

Decay time	Exp. value (s)
$\tau_1$	$(2.9 \pm 0.6)$
$\tau_2$	$(47 \pm 2)$
$\tau_3$	$(475 \pm 5)$

Table S2: Characteristic decay times obtained from the fit of the cooling data.

In order to substantiate this interpretation, we have performed a COMSOL simulation of our devices. In Fig. S4(a) we show the triangular mesh utilized for the simulation, and in Fig. S4(b) a zoom-in of the top part. The simulation has been performed assuming a step-like increase of the temperature of the top layer by 2 K from room temperature ( $T_0 = 303$  K).

Figure S5(a) shows the temperature distribution at  $t \simeq 0$  when the device is at 303 K, except for the topmost layer to which just a temperature jump of 2 K has been applied. Figure S5(b) shows the temperature distribution after  $0.1 \mu\text{s}$ . Figures S6(a) and (b) show a zoom-in of the starting ( $t = 1$  ns) and final temperature distribution, respectively. We can see that the upper layers of the sample, including the  $\text{SiO}_2$  layer, rapidly thermalize in a time much shorter than our measurement time, while the thick Si substrate heats up with a much longer characteristic time. These results support our description of the thermal behaviour of the device. Therefore, the relevant thermalization time between sample and sensor, which we use in the paper, is  $\tau = \tau_1 = (2.9 \pm 0.6)$  s.

Based on the above results, we include Ti-MLG, Au, Ti, and  $\text{SiO}_2$  in the following total heat capacity calculation. For a surface area of  $A = 5.10 \text{ mm} \times 5.95 \text{ mm} = 30.345 \text{ mm}^2$ , and from the well known densities ( $\rho$ ) and specific heat capacities ( $c$ ) of Au, Ti, and  $\text{SiO}_2$

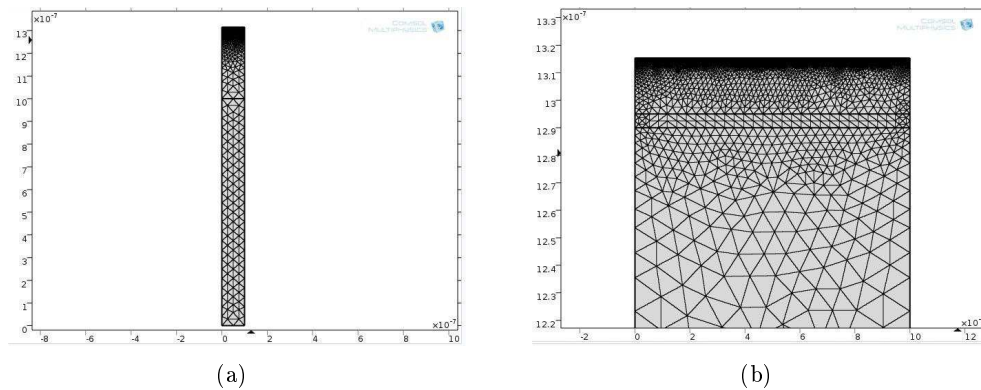


Figure S4: (a) Evaluation mesh (free Triangular with a Normal Size) utilized in the COMSOL simulation. (b) Zoom-in of the top part of the sample.

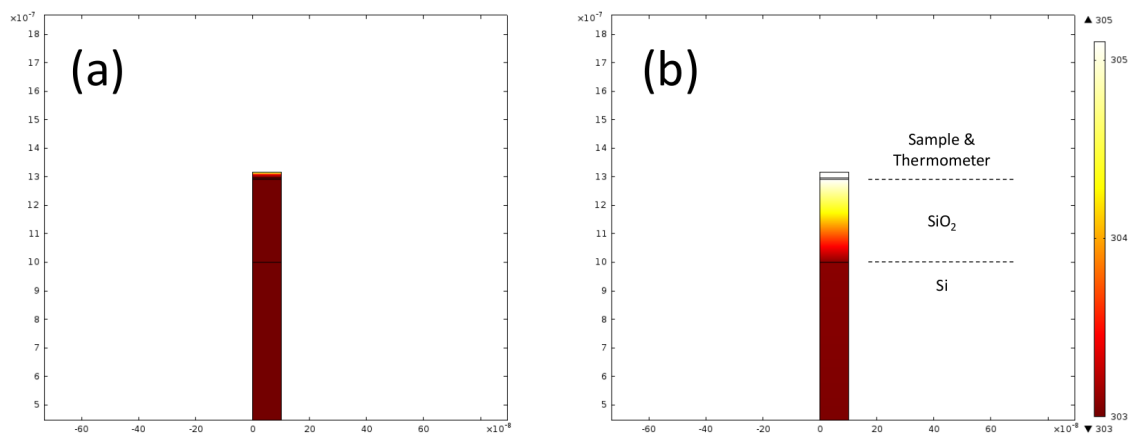


Figure S5: (a) Temperature distribution at  $t = 1$  ns when the temperature jump of 2 K has just been applied to the topmost layer of the stack. All other parts of the stack are still at 303 K. (b) Temperature distribution at  $t = 0.1 \mu s$ .

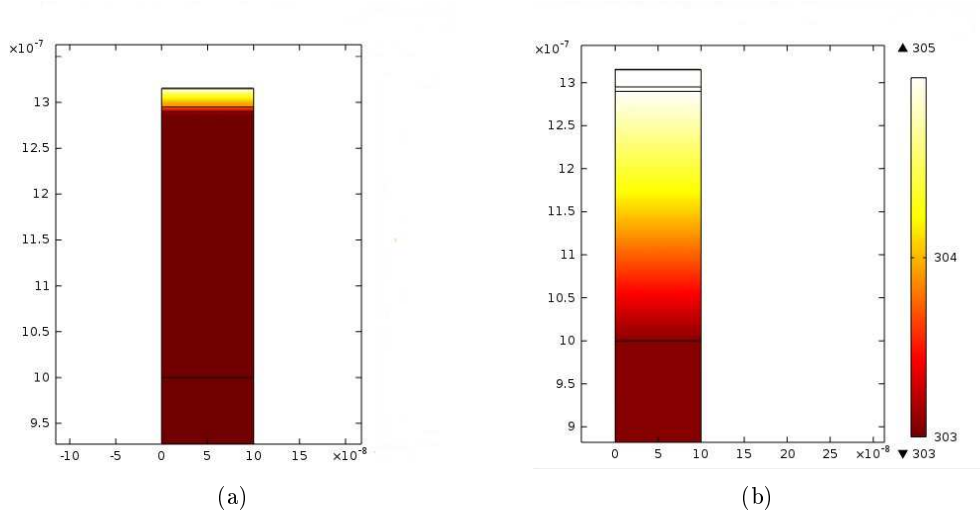


Figure S6: (a) Zoom-in of the temperature distribution at  $t = 1$  ns. (b) Zoom-in of temperature distribution at  $t = 0.1 \mu\text{s}$ .

[3] we can calculate the heat capacity of each layer. As an example we obtain for gold:

$$\begin{aligned}
 C_{Au} &= A \cdot d \cdot \rho_{Au} \cdot c_{Au} = \\
 &= 30.345 \text{ mm}^2 \cdot 20 \cdot 10^{-6} \text{ mm} \cdot 19.3 \cdot 10^{-3} \text{ g/mm}^3 \cdot 0.129 \text{ J/(K} \cdot \text{g)} = \\
 &= (1.51 \pm 0.02) \cdot 10^{-6} \text{ J/K}
 \end{aligned}$$

where  $d$  is the gold layer thickness. Similarly we obtain  $C_{Ti} = (0.36 \pm 0.01) \cdot 10^{-6} \text{ J/K}$  and  $C_{SiO_2} = (13.12 \pm 0.13) \cdot 10^{-6} \text{ J/K}$ . On the other hand,  $C_{graphene} \sim 10^{-8} \text{ J/K}$  [6], and the contribution of the Ti deposited on the MLG (a few ML) is negligible ( $C \sim 5 \cdot 10^{-8} \text{ J/K}$ ), and therefore we can neglect the contribution of the sample (Ti-MLG) in the total heat capacity calculation. We get as the final result  $C = (14.99 \pm 0.17) \cdot 10^{-6} \text{ J/K}$ .

## References

- [1] Andrea C. Ferrari, J.C. Meyer, V. Scardaci, C. Casiraghi, Michele Lazzeri, Francesco Mauri, S. Piscanec, Da. Jiang, K.S. Novoselov, S. Roth, et al. Raman spectrum of graphene and graphene layers. *Physical Review Letters*, 97(18):187401, 2006.
- [2] Fred Lacy. Developing a theoretical relationship between electrical resistivity, temperature, and film thickness for conductors. *Nanoscale Research Letters*, 6(1):636, 2011.
- [3] David R. Lide. *CRC Handbook of Chemistry and Physics*. CRC Press, 84th edition, 2007.
- [4] L.M. Malard, M.A. Pimenta, G. Dresselhaus, and M.S. Dresselhaus. Raman spectroscopy in graphene. *Physics Reports*, 473(5–6):51–87, 2009.
- [5] Raymond Serway and John Jewett. *Principles of physics: a calculus-based text*. Brooks Cole, Pacific Grove, USA, 5th edition, 2012.
- [6] Ji Won Suk, Karen Kirk, Yufeng Hao, Neal A. Hall, and Rodney S. Ruoff. Thermoacoustic sound generation from monolayer graphene for transparent and flexible sound sources. *Advanced Materials*, 24(47):6342–6347, 2012.